Chapter5

Investigation of photocatalytic efficiency of metal-non-metal (Fe-B) co-doped ZnS.

5.1 Introduction

ZnS is an eco-friendly material as it is compatible with living organisms providing a broad range of daily applications without any toxic effect on human health and the environment. Along with this, it has a great efficiency for the removal and complete degradation of environmental pollutants. ZnS offers a high driving force due to its unique chemical and physical properties for reduction and oxidation processes in dye degradation.[1–4]

Co-doping of metal-non-metal may additionally improve photocatalytic activities of ZnS by narrowing the band-gap energy of Zinc Sulfide and reducing electron-hole recombination. Oxides and sulfides of metals are considerably used as photocatalytic semiconductors for decades. Zinc Sulphide is one of the broadly used semiconductors. It exists in cubic (zinc blende) and hexagonal (wurtzite) forms. Despite this, very little research has been reported on non-metal doping. Recently, Madhuri MB reported the photocatalytic activity of Cd and N co-doped ZnS into the Zinc Sulphide crystals.[5–7] Vijaya Kumari et.al reported one fold modification of ZnO with non-metal ions such as C, N, S co-doped ZnO or C, N co-doped ZnS photocatalysts.[8–11]

Hence, it is important to design and explore non-metal-doped ZnS-based photocatalysts. Recently, carbon materials such as graphene and carbon dots have been widely established as effective photosensitizers in catalytic ozonization and photocatalytic processes due to their high mobility of photo-produced electrons. They established that the conjugated π structure of carbon is appropriate for the improved interactivity of composites between carbon and semiconductors.[12–16]To further enhance the electron transfer and range the visible light harvesting region, carbon-doped with N atoms can regulate the work function of carbon and induce charge delocalization.[17] Hsu et al. have developed that sandwich-like hydrogenated-doped anatase TiO_2 nanocrystals/N-doped carbon dots@layer/rutile TiO_2 nanorod arrays have exhibited efficient photoelectron-chemical activity of water oxidation.[18] ZnS having a sulfur-vacancy defect and N-doped carbon-coated (ZnS@N-C)was achieved for the visible-light-driven photodegradation of tetracycline hydrochloride (TCH). The acquired ZnS@N-C exhibited enhanced photocatalytic activity compared with ZnS for TCH removal.[19,20]

Hence, inspired by the literature we established a Fe and B co-doped catalytic system for efficient dye degradation. To the best of our knowledge, there are no reports on photocatalytic degradation having B and Fe metals in the ZnS system.

5.2 Synthesis of catalyst

Materials and Methods

Zinc acetate dihydrate ($(CH_3COO)_2Zn.2H_2O$) AR grade sigma Aldrich, $FeCl_2.4\ H_2O$, and Boric Acid (H_3BO_3) were used as dopants. Sodium hydroxide (NaOH) AR grade Merck, Sodium sulfide ($Na_2S.xH_2O$), 2-Mercaptoehanol ($HSCH_2CH_2OH$), Rhodamine B ($C_{28}H_{31}ClN_2O_3$) S.D. fine chemicals.

All reagents were used without any further purification. 2- Mercaptoethanol was used as a capping agent. 5×10^{-3} mol of Zinc acetate was dissolved in 200 ml D.I water. 50 ml of each dopant (11.49×10^{-5}mol, for $Fe_{0.07}$ mol and 3.69×10^{-4}mol for $B_{0.07}$ and (8.19×10^{-5}mol, for $Fe_{0.05}$ and 2.64×10^{-4}mol for $B_{0.05}$) were added dropwise under vigorous stirring. Stirring was continued for 30min until complete dissolution of both dopants. During the experiment, the pH of the solution was maintained at 11 using an aqueous solution of NaOH (1M), followed by dropwise addition of 2-mercaptoethanol (5×10^{-3} mol in 50 ml). The temperature of the reaction mixture was gradually raised to 70°C. The reaction mixture was stirred thoroughly for a further half an hour to obtain a homogenous mixture. To this Na_2S solution, (5×10^{-3} mol in 50 ml) was added dropwise at the rate of 1mL /min. The reaction mixture was further stirred for 3hr to obtain homogenous stabilized dispersion and then allowed to cool naturally. The mixture was centrifuged at 6000 rpm for 5 min and washed with DI water 4 times and finally with absolute alcohol to remove impurities. The resulting precipitate was dried at 60°C. Pristine ZnS was also synthesized by the same method without using dopants.

5.3 Characterization

X-Ray powder sample diffraction(XRD) patterns of samples were obtained by X-ray Diffractometer (Panalytical X Pert Pro) with Cu Kα radiation, λ= 0.15418nm,100 kV. Scanning electron microscopy (SEM, Quanta 200FEG) was employed to confirm the size and morphology of the nanoparticles. The samples were degassed at 80°C preceding to Brunauer-Emmett-Teller(BET) measurements. The BET surface area (SBET) was calculated by nitrogen adsorption (Micrometrics ASAP 2020, USA) via a multipoint BET method using the adsorption data in the relative(P/P_o) range of 0.0-1.0. The porosity of prepared samples was evaluated by desorption isotherms using the Barret-Joyner-Halender (BJH) method.

Chemical composition analysis of all the samples was done by the EDAX technique (JEOL 8086). A vibrating sample magnetometer (VSM) analysis was carried out for the study of the magnetic behavior of synthesized samples at room temperature under applied magnetic fields up to 15000 Oe.

5.4 Results and Discussion

The XRD pattern of all synthesized Co-doped ZnS NPs manifests three predominant diffraction peaks corresponding to the (111), (220), and (311) planes respectively which are in good agreement with the standard diffraction peaks (JCPDS 00-001-0792) of cubic structure (Fig. 5.1 A and B).

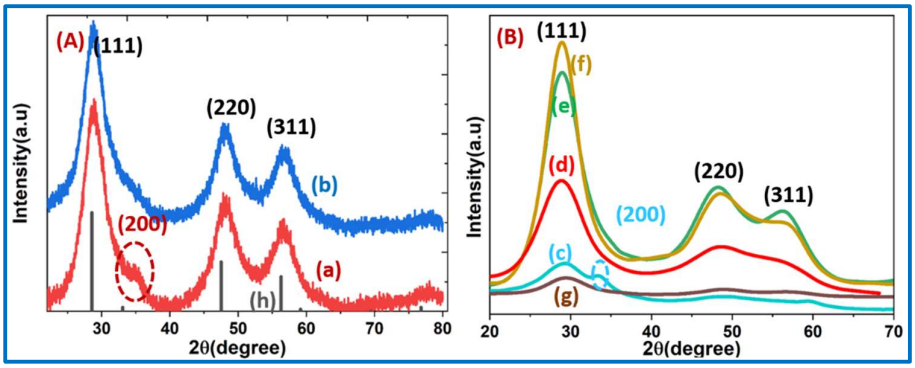

Fig. 5.1A PXRD of synthesized co-doped NPs with (a) $Zn_{1-0.14}Fe_{0.07}B_{0.07}S$ (b) $Zn_{1-0.10}Fe_{0.05}B_{0.05}S$ and Fig. 5.1 B PXRD of synthesized mono-doped NPs with (c) $Zn_{1-0.07}Fe_{0.07}S$ (d) $Zn_{1-0.05}Fe_{0.05}S$ (e) $Zn_{1-0.07}B_{0.07}S$ (f) $Zn_{1-0.05}B_{0.05}S$ (g) Pristine ZnS (h) Bulk ZnS.

These results suggested clearly that substitutional doping does not affect the crystal structure significantly. No additional peak except $Fe_{0.07}B_{0.07}$ and $Fe_{0.07}$ was observed in the XRD pattern which means all samples were in a pure phase. The mean crystallite size of nanoparticles was calculated using the Debye-Scherrer equation (Eq(1)),[21]

$$D = \frac{0.94}{\beta cos\theta} \qquad (1)$$

Here, D is the crystallite size, λ, the wavelength of X-Rays (1.54056A°), β ,the full width at the half maxima(in rad) and θ the Bragg's angle.

Energy dispersive spectra (EDS) were recorded at room temperature for the chemical composition analysis shown in (Fig. 5.2 a-f). EDS spectra reveal that targeted dopants successfully doped into the ZnS matrix.

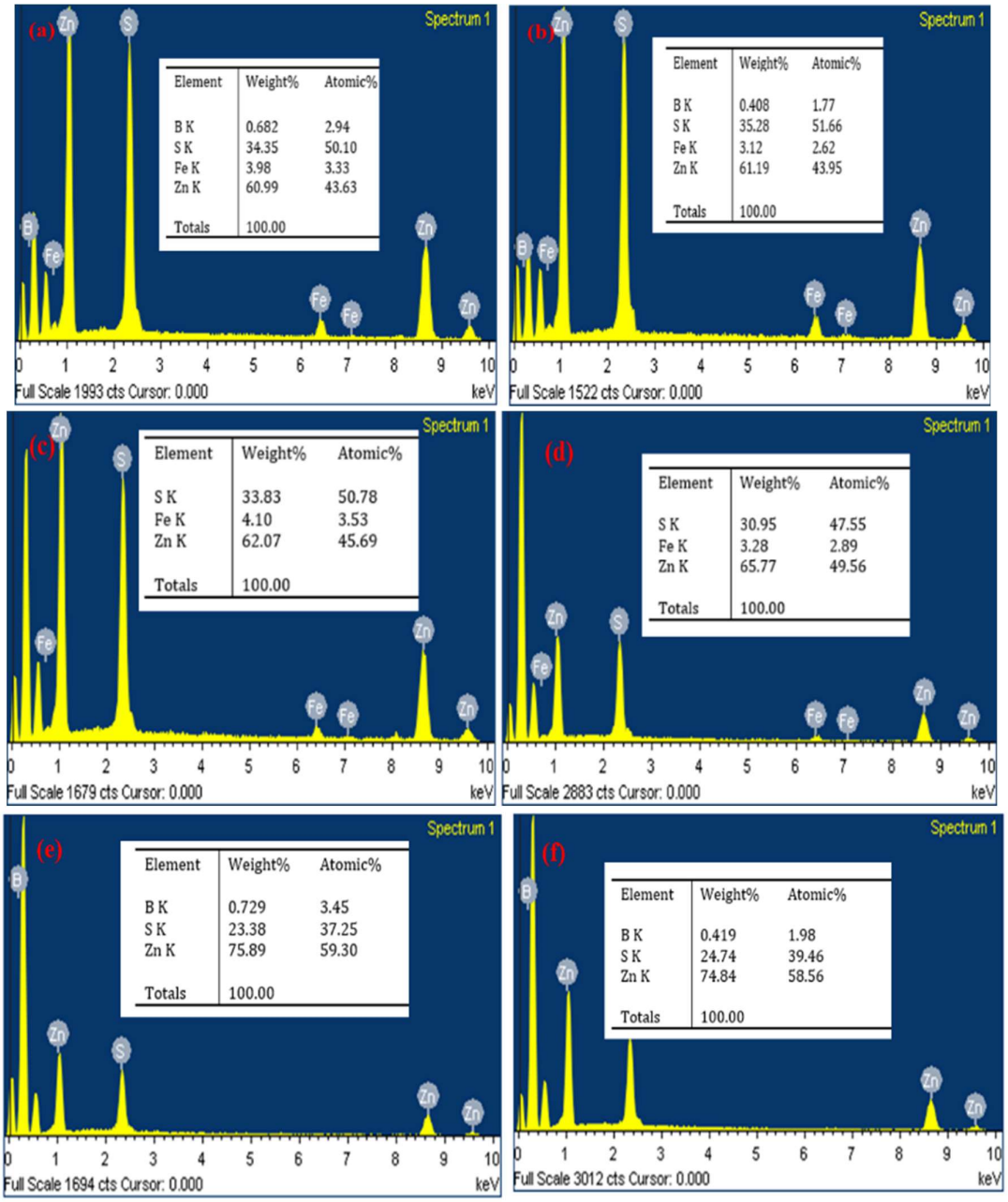

Fig. 5.2 EDX spectra of synthesized (a) $Zn_{1-0.14}Fe_{0.07}B_{0.07}S$ (b) $Zn_{1-0.10}Fe_{0.05}B_{0.05}S$ (c) $Zn_{1-0.07}Fe_{0.07}S$ (d) $Zn_{1-0.05}Fe_{0.05}S$ (e) $Zn_{1-0.07}B_{0.07}S$ (f) $Zn_{1-0.05}B_{0.05}S$ (g) Pristine ZnS nanoparticles.

Table 5.1 Absorption edge, Bandgap, Crystallite sizes, and surface charge of synthesized ZnS NPs.

S. No.	ZnS NPs	Absorption edge (nm)	Band-gap (eV)	Scherrer (nm)
1.	Bulk	337	3.66	-
2.	$Zn_{1-0.14}Fe_{0.07}B_{0.07}S$	322	4.31	1.85
3.	$Zn_{1-0.10}Fe_{0.05}B_{0.05}S$	454	4.12	1.58
4.	$Zn_{1-0.07}Fe_{0.07}S$	310	4.08	1.90
5.	$Zn_{1-0.05}Fe_{0.05}S$	313	4.05	3.00
6.	$Zn_{1-0.07}B_{0.07}S$	322	4.11	1.92
7.	$Zn_{1-0.05}B_{0.05}S$	316	4.02	3.07
8.	Pristine	315	3.93	2.45

SEM Images with elemental Mapping were performed using a Gold grid for structural and morphological study (Fig. 5.3A (a-e), Fig. 5.3B (a-e) and Fig. 5.3C (a-d)). SEM images indicate spherical shapes for all co-doped synthesized NPs.

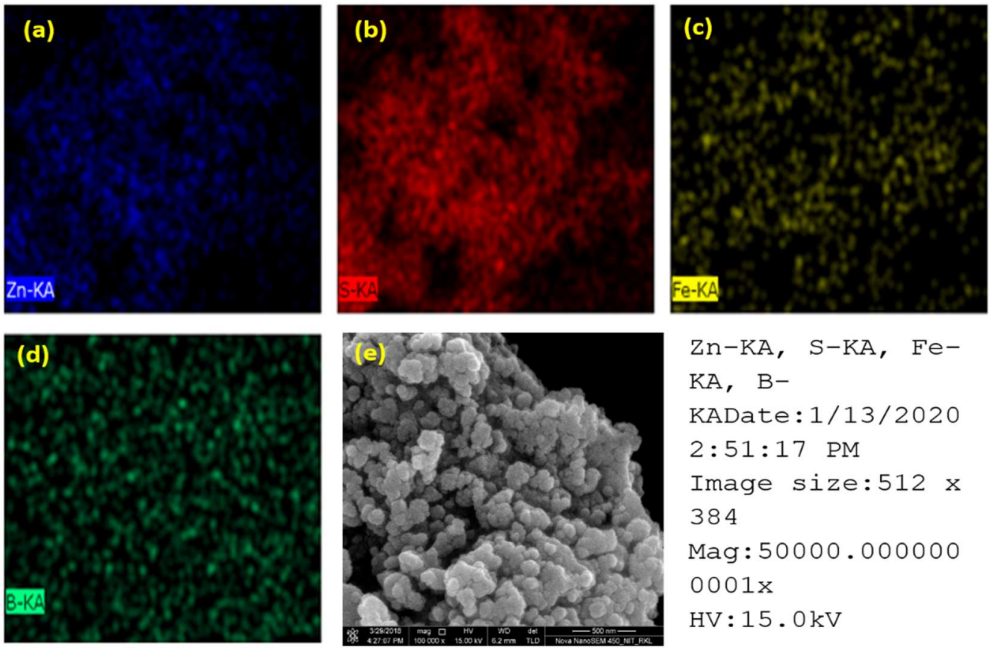

Fig. 5.3A SEM image of co-doped synthesized $Zn_{1-0.14}Fe_{0.07}B_{0.07}S$ with elemental Mapping of (a) Zn (Blue), (b) S (red), (c)Fe (yellow) and (d) B (green) (e) SEM

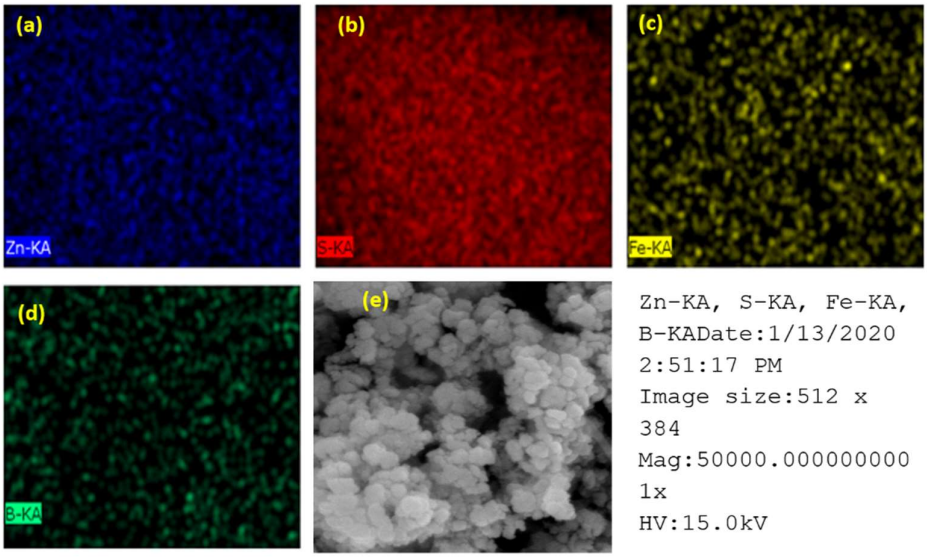

Fig. 5.3 B SEM image of co-doped synthesized $Zn_{1-0.10}Fe_{0.05}$ $B_{0.05}S$ with elemental Mapping of (a) Zn (Blue), (b) S (red), (c)Fe (yellow) and (d) B (green). (e) SEM

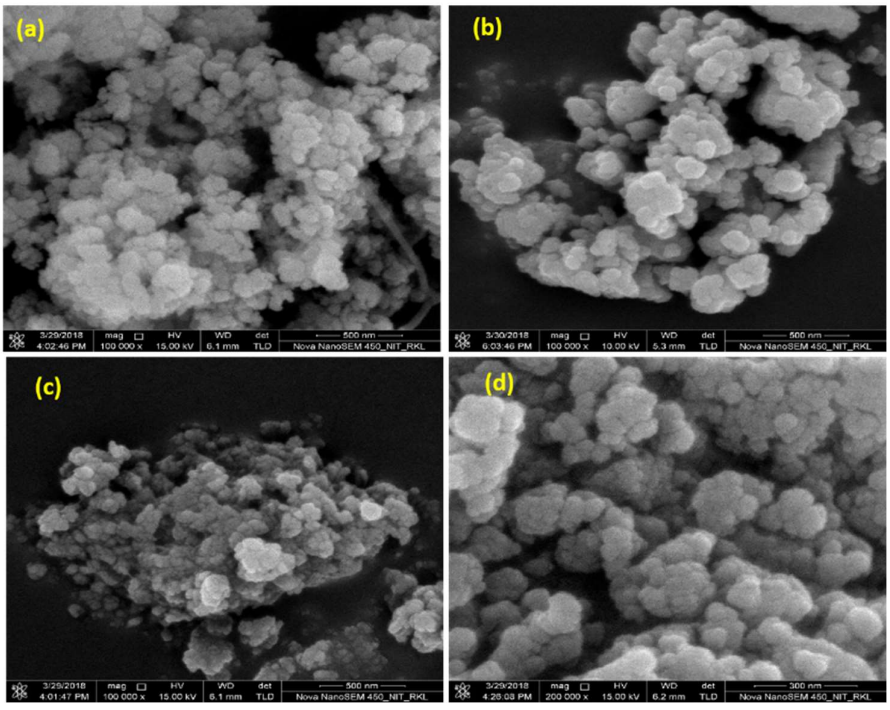

Fig. 5.3 C SEM image of mono doped ZnS NPs (a) $Zn_{1-0.07}Fe_{0.07}S$ (b) $Zn_{1-0.05}Fe_{0.05}S$ (c) $Zn_{1-0.07}B_{0.07}S$ (d) $Zn_{1-0.05}B_{0.05}S$.

To further confirmed the morphology and crystallographic features, HRTEM analysis was carried out. HRTEM images clearly show the morphology of as-synthesized samples was spherical. An agglomeration was also seen in samples (Fig. 5.4 A-F).

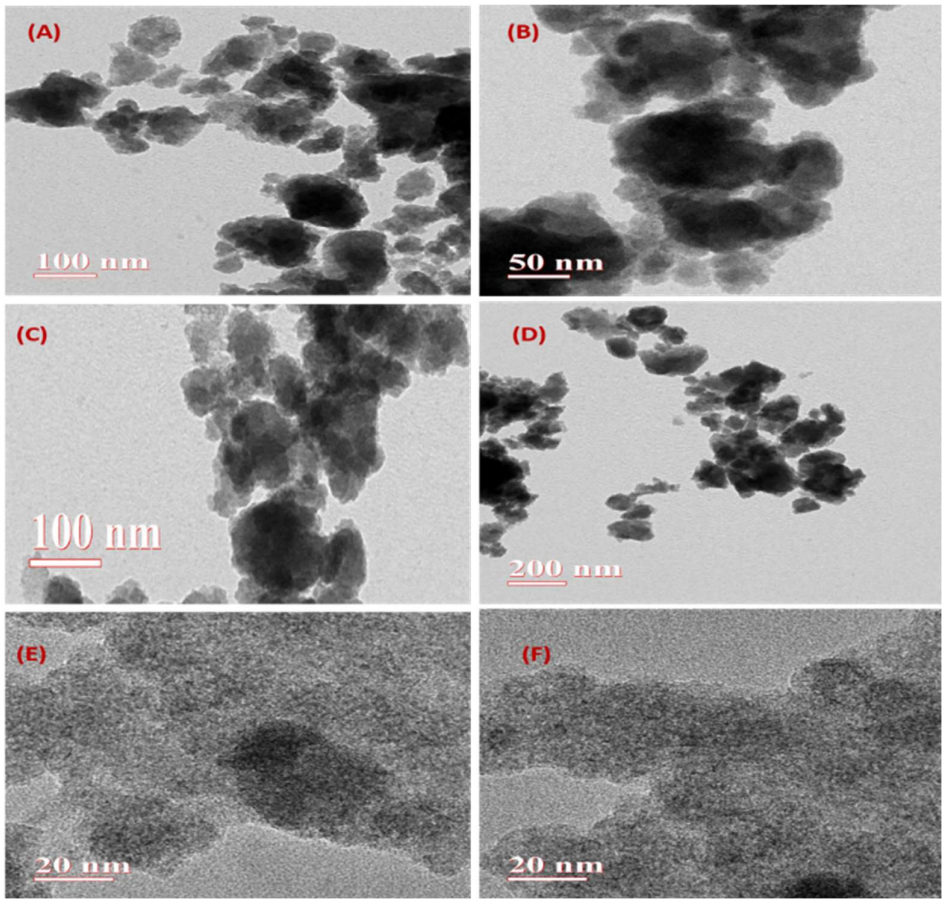

Fig. 5.4 TEM analysis of synthesized ZnS NPs (A) $Zn_{1-0.14}Fe_{0.07}B_{0.07}S$ (B) $Zn_{1-0.10}Fe_{0.05}B_{0.05}S$ (C) $Zn_{1-0.07}Fe_{0.07}S$ (D) $Zn_{1-0.05}Fe_{0.05}S$ (E) $Zn_{1-0.07}B_{0.07}S$ (F) $Zn_{1-0.05}B_{0.05}S$.

UV- Visible absorption spectra of co-doped ZnS NPs is recorded in the range of 200-400 nm. The strongest excitonic absorption peak was observed in the range of 286- 295nm (Fig.5.5 A and B). The optical direct bandgap is determined by tauc relationship by extrapolating the straight-line portion to the hν-axis[Eq. (6)][22]

$$(\alpha h\nu)^2 = B(h\nu - E_g) \quad (6)$$

Where, $(h\nu)$ is the photon energy, and α, the absorption coefficients($\alpha = 4\pi\kappa/\lambda$, κ is absorption, λ is the wavelength in nm), and A , a constant.

The obtained values of energy band-gaps are given in (Table 5.1, shown in Fig. 5.6 a-g). A comparison with values of band-gap between bulk and co-doped synthesized Nps can be seen,

band-gap increases with increasing dopant contents. This is due to the discreteness of the bands with decreasing particle size.[23]

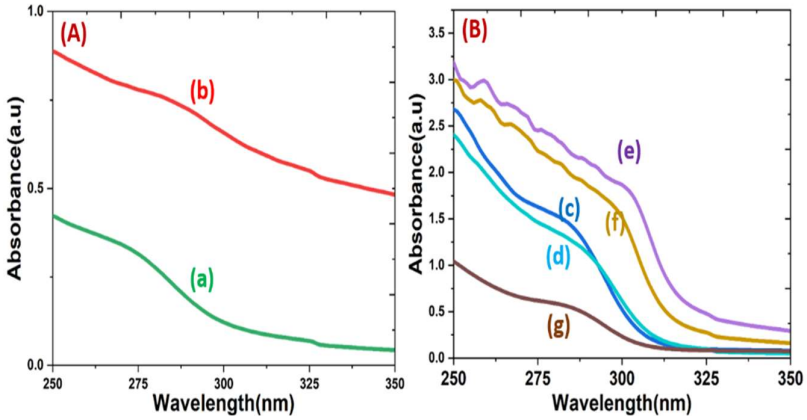

Fig. 5.5 (A) UV analysis of synthesized ZnS NPs (a) $Zn_{1-0.14}Fe_{0.07}B_{0.07}S$ (b) $Zn_{1-0.10}Fe_{0.05}B_{0.05}S$ and Fig. 5.5 (B) (c) $Zn_{1-0.07}Fe_{0.07}S$ (d) $Zn_{1-0.05}Fe_{0.05}S$ (e) $Zn_{1-0.07}B_{0.07}S$ (f) $Zn_{1-0.05}B_{0.05}S$ (g) pristine.

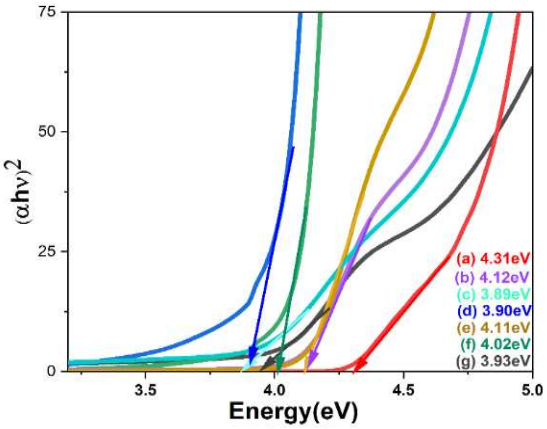

Fig. 5.6 Plot of $(\alpha h\nu)^2$ vs hν of (a) $Zn_{1-0.14}Fe_{0.07}B_{0.07}S$ (b) $Zn_{1-0.10}Fe_{0.05}B_{0.05}S$ (B) (c) $Zn_{1-0.07}Fe_{0.07}S$ (d) $Zn_{1-0.05}Fe_{0.05}S$ (e) $Zn_{1-0.07}B_{0.07}S$ (f) $Zn_{1-0.05}B_{0.05}S$ (g) pristine.

Fig.5.7 shows room temperature PL spectra of as-synthesized co-doped nanoparticles capped by 2-mercaptoethanol under 295 nm excitation. The emission at 415 nm is due to charge carrier recombination from Vs to VB, whereas the peak at 460 nm is due to the transfer of electron from V_{Vs} to V_{Zn}. The emission at 490 nm indicates the presence of superfluous Zn ions on the surface.[24]

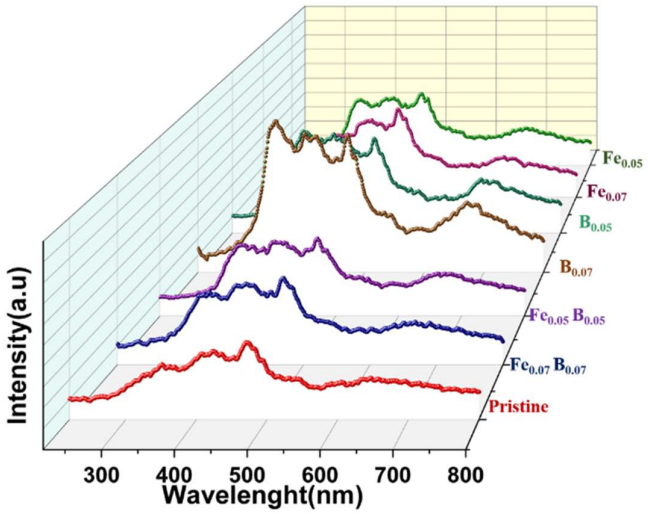

Fig. 5.7 Photoluminescence spectra of synthesized ZnS NPs.

Evaluation of photocatalytic activity

The photocatalytic performance of synthesized ZnS NPs.

The time-dependent photocatalytic activities of synthesized metal-non-metal co-doped ZnS samples are shown in Fig.5.8 A-H. Photocatalytic activity of co-doped synthesized NPs was evaluated spectrophotometrically in terms of change in absorption intensity (λ_{max} at 555nm) of RhB in an aqueous solution. The % decolorization efficiency of samples was calculated as Eq.7

$$\% \text{ Efficiency} = 100\times \frac{[A_o - A]}{A_o} = 100\times\frac{[C_o - C]}{C_o} \quad (7)$$

Where, A_o, A, C_o, and C are initial absorbance, absorbance after irradiation at various time intervals, initial concentration of the solution, and concentration of dye after irradiation at various time intervals, respectively. the PL spectra of illuminated basic solution of terephthalic acid in presence of $Fe_{0.05}B_{0.05}$ doped ZnS NPs at different time intervals were recorded (Fig.5.9A). The PL intensity at 425 nm increases with irradiation time in presence of ZnS:Fe and the pristine ZnS NPs. This observation confirms that ·OH actively takes part in the degrada- tion of RhB dye in aqueous solution.[25–27]

The plot of ln C_o/C_t vs irradiation time is a straight line and passes through the origin (Fig. 5.9(B)) indicating the first-order decay kinetics. The values of the rate constant for all co-doped ZnS samples are given in Table5.2.

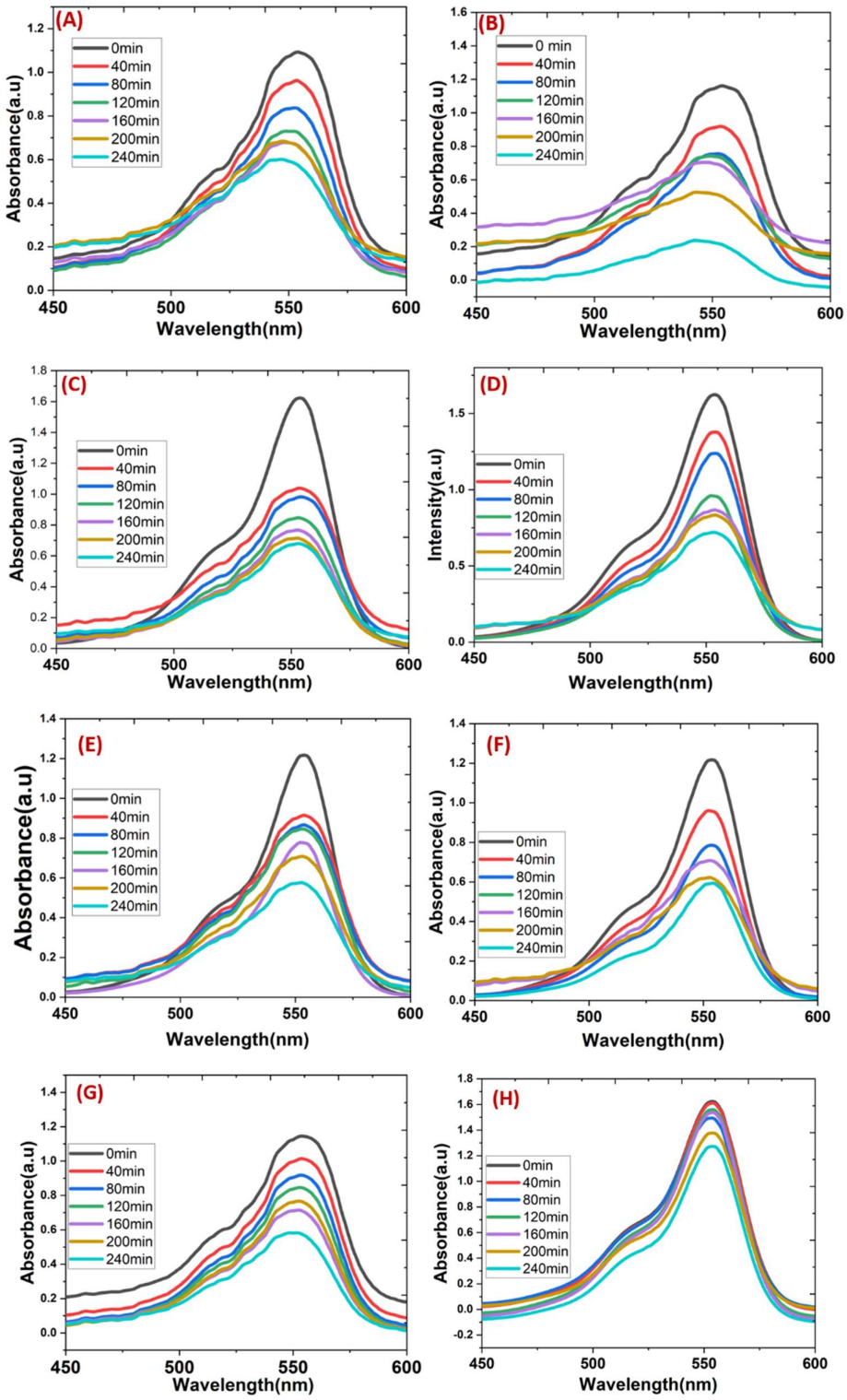

Fig. 5.8 Photocatalytic degradations of RhB dye in terms of diminishing intensity of λ max at 554nm in presence of (A) $Zn_{1-0.14}Fe_{0.07}B_{0.07}S$ (B) $Zn_{1-0.10}Fe_{0.05}B_{0.05}S$ (C) $Zn_{1-0.07}Fe_{0.07}S$ (D) $Zn_{1-0.05}Fe_{0.05}S$ (E) $Zn_{1-0.07}B_{0.07}S$ (F) $Zn_{1-0.05}B_{0.05}S$ (G) Pristine (H) Without catalyst.

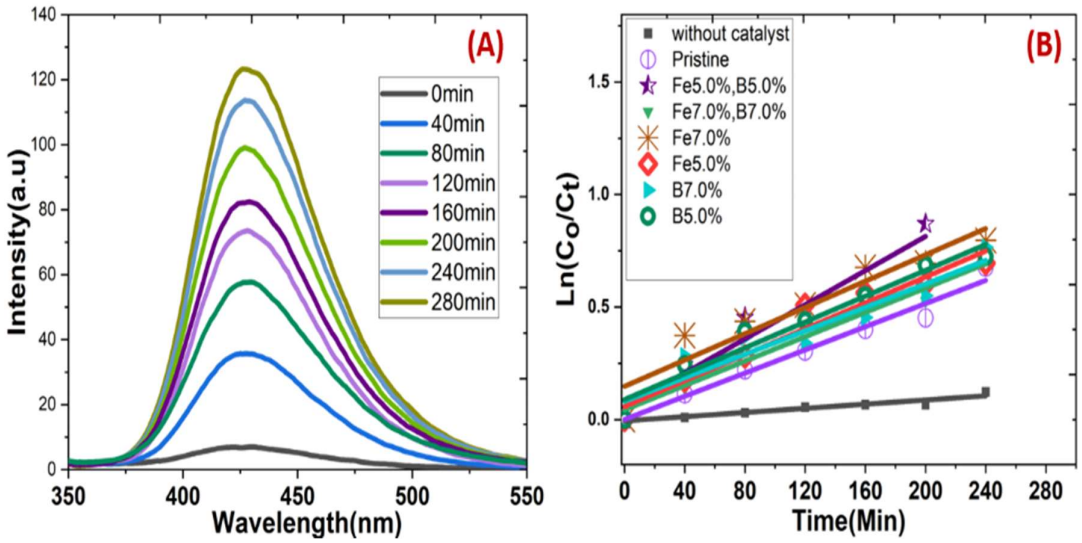

Fig.5. 9(A) PL intensity of basic solution of terephthalic acid under HPMV irradiation at different time intervals in presence of ZnS: $Fe_{0.05}B_{0.05}$ NPs. (B)Photo-degradation of RhB under HPMV irradiation.

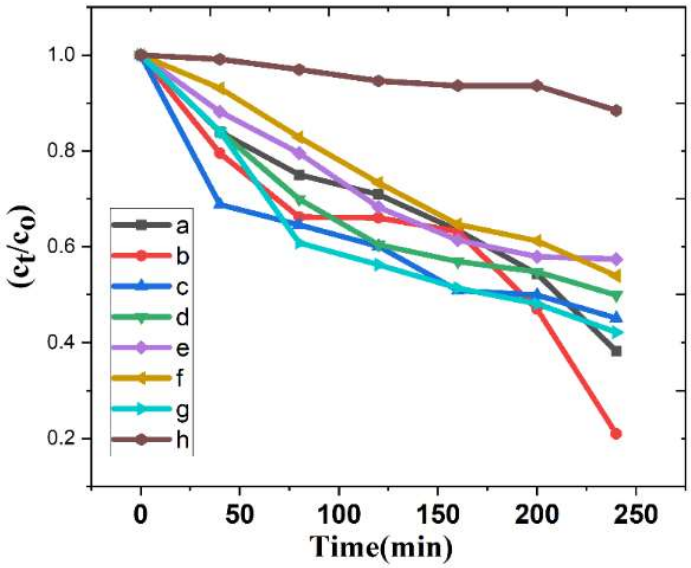

Fig.5.10 Photodegradation of RhB under HPMV irradiation in precence of (a) $Zn_{1-0.14}Fe_{0.07}Ni_{0.07}S$ (b) $Zn_{1-0.10}Fe_{0.05}Ni_{0.05}S$ (c) $Zn_{1-0.07}Fe_{0.07}S$ (d) $Zn_{1-0.05}Fe_{0.05}S$ (e) $Zn_{1-0.07}B_{0.07}S$ (f) $Zn_{1-0.05}B_{0.05}S$ (g) pristine (h) without any catalyst.

Table 5.2 Degradation of an aqueous solution of RhB dye under white light irradiation after 4.33hr.

samples	% Degradation	Rate constant (h^{-1})	correlation coefficient R^2
$Zn_{1-0.14}Fe_{0.07}B_{0.07}S$	61.82	0.2408	0.9327
$Zn_{1-0.10}Fe_{0.05}B_{0.05}S$	79.06	0.3909	0.9013
$Zn_{1-0.07}Fe_{0.07}S$	54.91	0.1839	0.9706
$Zn_{1-0.05}Fe_{0.05}S$	50.09	0.1605	0.9368
$Zn_{1-0.07}B_{0.07}S$	46.05	0.1543	0.9554
$Zn_{1-0.05}B_{0.05}S$	42.57	0.1387	0.9935
Pristine	44.23	0.1349	0.9228
Without catalyst	13.66	0.03	0.939

Room temperature vibrating sample magnetometer (VSM) study of pristine, mono-doped, and co-doped ZnS was carried out. Fig. 5.11 (A-C) displays the plot between the applied magnetic field and magnetic moment curves. The negative slope of the M-H curve in Fig. 5.11A (inset) asserts the diamagnetic behavior of pristine ZnS nanoparticles.

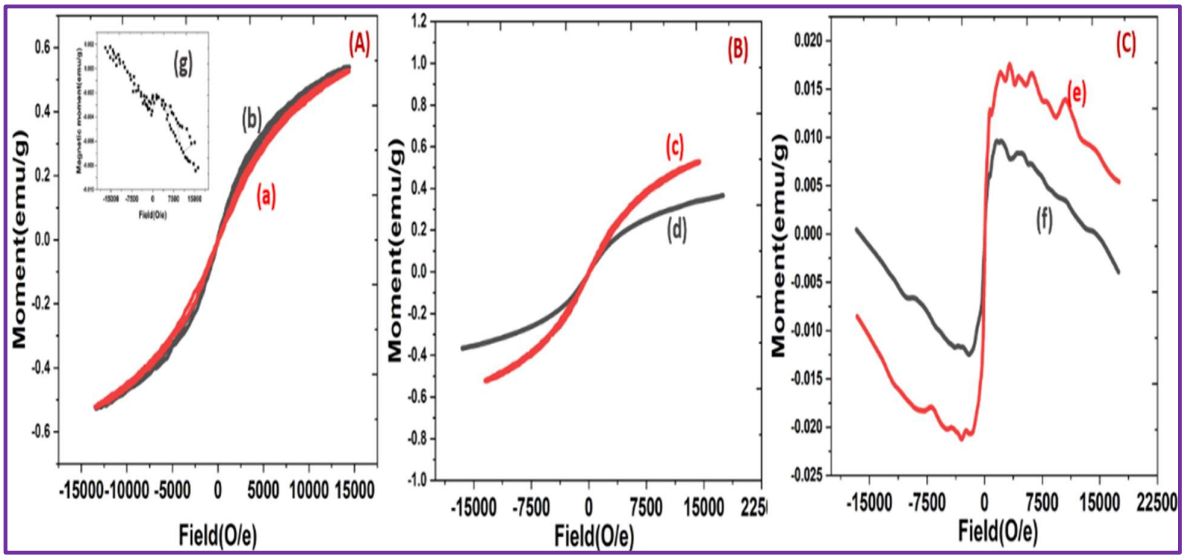

Fig.5.11. VSM Hysteresis curves for (A) (a) $Zn_{1-0.14}Fe_{0.07}B_{0.07}S$ (b) $Zn_{1-0.10}Fe_{0.05}B_{0.05}S$ (inset; pristine ZnS) (B) (c) $Zn_{1-0.07}Fe_{0.07}S$ (d) $Zn_{1-0.05}Fe_{0.05}S$ (C) (e) $Zn_{1-0.07}B_{0.07}S$ (f) $Zn_{1-0.05}B_{0.05}S$.

Table 5.4 The VSM data of synthesized ZnS NPs at room temperature with different amounts of dopants. (Maximum field 15000 O/e)

Sample	Susceptibility χ 10^{-3}	Retentivity (emu/g) 10^{3}	Ms(emu/g) 10^{-3}	Coercivity(Oe)
Pristine	-0.000097	0.11	1.22	2211.0
$Zn_{1-0.14}Fe_{0.07}B_{0.07}S$	0.0035	7.02	525.00	54.80
$Zn_{1-0.10}Fe_{0.05}B_{0.05}S$	0.0035	7.49	532.95	50.74
$Zn_{1-0.07}Fe_{0.07}S$	0.1003	3.39	360.00	4.40
$Zn_{1-0.05}Fe_{0.05}S$	0.2753	11.84	1010	56.36
$Zn_{1-0.07}B_{0.07}S$	0.0069	1.55	25.51	0.81
$Zn_{1-0.05}B_{0.05}S$	0.0052	2.29	19.25	320.83

The electrochemical analyses were carried out to understand the effect of dopant ions on the redox behavior of the material.[28–30] The CV curves (Fig. 5.12 A) show the anodic current at negative potential. Electrochemical impedance spectral (EIS) measurements (Fig. 5.12 B) were performed to study the conducting behaviour of the material. From the impedance spectra, it can be observed that $B_{0.05}$ has the highest conductivity.

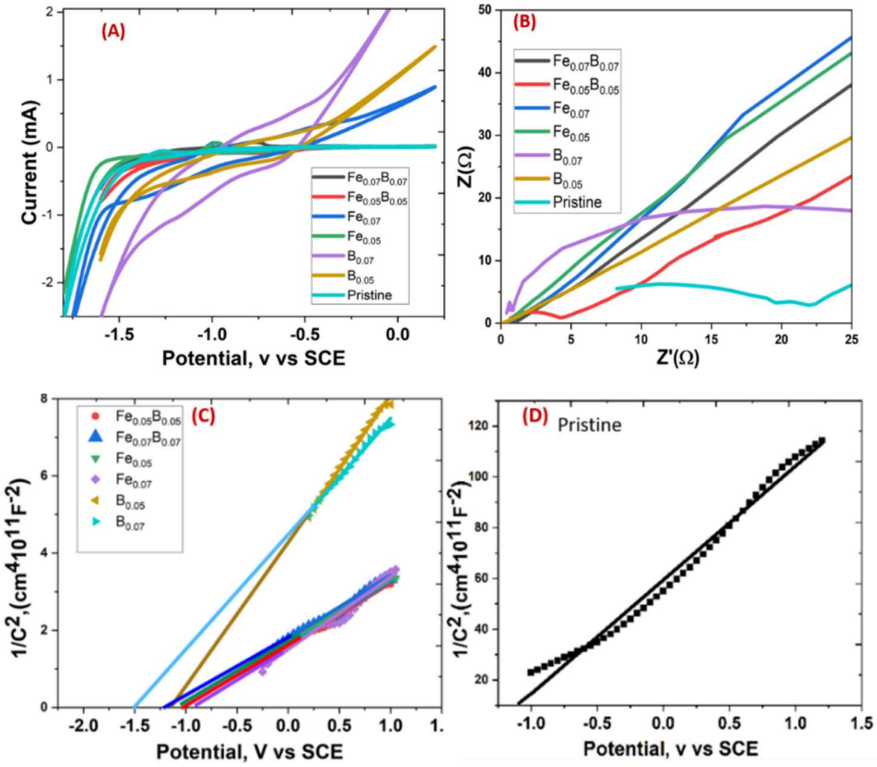

Fig. 5.12 (A) Cyclic voltammogram of synthesized ZnS Nps as a working electrode in aqueous solution, (B) EIS Nyquist plots (C) Normalized Mott–Schottky plot (D) Mott-Schottky of Pristine ZnS. (Scan rate: 25 mV/Sec. RE = saturated calomel electrode (SCE), CE = platinum wire).

Mott–Schottky (MS) (Fig. 5.12 C, Table 5.5, 5.6) measurements were carried out to trace the origin and fate of charge carriers in the material. The positive slope indicates the n-type semiconductor nature of all the synthesized samples, the highest donor density was observed in $Fe_{0.05}$. This requires less potential bias to achieve the Fermi level from the depletion region.

Table 5.5 MS and EIS data of synthesized ZnS NPs.

samples	Conductivity (10^{-6} S/cm)	Donor density (N_d)/cm^{-3} 10^{20}
$Zn_{1-0.14}Fe_{0.07}B_{0.07}S$	69.03	1.01
$Zn_{1-0.10}Fe_{0.05}B_{0.05}S$	47.19	1.01
$Zn_{1-0.07}Fe_{0.07}S$	189.7	0.88
$Zn_{1-0.05}Fe_{0.05}S$	203.4	1.02
$Zn_{1-0.07}B_{0.07}S$	34.00	0.54
$Zn_{1-0.05}B_{0.05}S$	256.14	0.43
Pristine	3.70	0.03

Table 5.6 Electronic band structure of the photocatalyst.

Samples	The slope from the MS plot (10^{11})	E_{cb}~ E_{fb} vs. SCE V	E_{cb}~ E_{fb} vs. NHE V	Band-gap energy eV	E_{VB} V
$Zn_{1-0.14}Fe_{0.07}B_{0.07}S$	1.63	-1.20	-0.95	4.31	+3.11
$Zn_{1-0.10}Fe_{0.05}B_{0.05}S$	1.64	-1.02	-0.77	4.12	+3.10
$Zn_{1-0.07}Fe_{0.07}S$	1.87	-0.91	-0.66	3.89	+2.98
$Zn_{1-0.05}Fe_{0.05}S$	1.62	-1.07	-0.82	3.90	+2.83
$Zn_{1-0.07}B_{0.07}S$	3.05	-1.50	-1.25	4.11	+2.61
$Zn_{1-0.05}B_{0.05}S$	3.83	-1.41	-1.16	4.02	+2.61
Pristine	44.88	-1.92	-1.67	3.93	+2.01

5.5 Conclusion

In this study pristine zinc sulfide, Fe-mono-doped, B- mono-doped, Fe-B metal-non-metal co-doped zinc sulfide have been synthesized successfully by the co-precipitation method.

The characterization of nanoparticles was done by using X-ray powder diffraction (XRD) and UV–VIS Spectroscopy, Fluorescence spectroscopy, EDS, SEM, and HRTEM analysis.

XRD results reveal that doping of boron merely adheres at the surface of ZnS, but Fe-doping at 7.0% in both mono-doped and co-doped ZnS distorts the ZnS cubic structure. Hence cubic phase has slightly shifted to the wurtzite phase.

Fe and B co-doping into ZnS exhibited a synergetic effect toward enhancing its photocatalytic activity. Whereas B mono-doped ZnS or Fe mono-doped system entraps the photo-excited electron at the conduction band of ZnS thereby minimizing electron-hole recombination.

A maximum decolorization of 79.85% was observed at 4.33hr under so UV light irradiation. The photocatalytic degradation of Rhodamine B using synthesized photocatalysts follows pseudo-first-order kinetics.

Since correlation coefficient $R^2 > 0.92$ it was found that all reactions found to follow pseudo-first-order kinetics. The synergistic effect between B-doped Fe-doped ZnS with sulfur-vacancy defects is accountable for the enhanced photocatalytic activity and stability. Efficient charge transfer and controlled electron-hole recombination are obtained at the interface of the Fe-B co-doped ZnS is a favorable strategy to enhance the photocatalytic efficiency of semiconductors.

5.6 References

(1) Ramasamy, V.; Praba, K.; Murugadoss, G. Synthesis and Study of Optical Properties of Transition Metals Doped ZnS Nanoparticles. *Spectrochim. Acta A Mol. Biomol. Spectrosc.* **2012**, *96*, 963–971.

(2) Kryshtab, T.; Khomchenko, V. S.; Andraca-Adame, J. A.; Rodionov, V. E.; Khachatryan, V. B.; Tzyrkunov, Y. A. The Influence of Doping Element on Structural and Luminescent Characteristics of ZnS Thin Films. Superlattices Microstruct. **2006**, *40*, 651–656.

(3) Zhang, Y.; Li, Y. Synthesis and Characterization of Monodisperse Doped ZnS Nanospheres with Enhanced Thermal Stability. **.** *Phys. Chem. B.* **2004**, *108* (46), 17805–17811.

(4) Lee, G. J.; Wu, J. J. Recent Developments in ZnS Photocatalysts from Synthesis to Photocatalytic Applications — A Review. *Powder Technol.* **2017**, *318*, 8–22.

(5) PB, M. M. and L. Effect of Cd and N Doping on Zinc Sulphide Nanoparticles Synthesised by Mechanochemical Method for the Photodegradation of Brilliant Green *Dye. Nano Res Appl.* **2019**, *5*, 1-5.

(6) Jiang, P.; Jie, J.; Yu, Y.; Wang, Z.; Xie, C.; Zhang, X.; Wu, C.; Wang, L.; Zhu, Z.; Luo, L. Aluminium-Doped n-Type ZnS Nanowires as High-Performance UV and Humidity Sensors. *J. Mater. Chem.* **2012**, *22*, 6856–6861.

(7) Yuan, G. D.; Zhang, W. J.; Zhang, W. F.; Fan, X.; Bello, I.; Lee, C. S.; Lee, S. T. P -Type Conduction in Nitrogen-Doped ZnS Nanoribbons. *Appl. Phys. Lett.* **2008**, *93* (21).

(8) Kumari, V.; Mittal, A.; Jindal, J.; Yadav, S.; Kumar, N. S-, N- and C-Doped ZnO as Semiconductor Photocatalysts: A Review. *Front. Mater. Sci.* **2019**, *13*, 1-21.

(9) Peng, H.; Liu, D.; Zheng, X.; Fu, X. N-Doped Carbon-Coated ZnS with Sulfur-Vacancy Defect for Enhanced Photocatalytic Activity in the Visible Light Region. *Nanomaterials* **2019**, *9*, 1657.

(10) Svob, L.; Thiandoume, C.; Lusson, A.; Bouanani, M.; Marfaing, Y.; Gorochov, O. P-Type Doping with N and Li Acceptors of ZnS Grown by Metalorganic Vapor Phase Epitaxy. *Appl. Phys. Lett.* **2000**, *76*, 1695–1697.

(11) Khan, M. S.; Shi, L.; Yang, X.; Ali, S.; Ullah, H.; Zou, B. Optoelectronic and Magnetic Properties of Mn-Doped and Mn-C Co-Doped Wurtzite ZnS: A First-Principles Study. *J. Condens. Matter Phys.* **2019**, *31*, 395702.

(12) Han, M.; Zhu, S.; Lu, S.; Song, Y.; Feng, T.; Tao, S.; Liu, J.; Yang, B. Recent Progress on the Photocatalysis of Carbon Dots: Classification, Mechanism and Applications. *Nano Today* **2018**, *19*, 201–218.

(13) Choi, J.; Kim, N.; Oh, J. W.; Kim, F. S. Bandgap Engineering of Nanosized Carbon Dots through Electron-Accepting Functionalization. *J Ind Eng Chem.* **2018**, *65*, 104–111.

(14) Jung, H. D.; Song, C. D.; Wang, S. Q.; Arai, K.; Wu, Y. H.; Zhu, Z.; Yao, T.; Katayama-Yoshida, H. Carrier Concentration Enhancement of P-Type ZnSe and ZnS by Codoping with Active Nitrogen and Tellurium by Using a δ-Doping Technique. *Appl. Phys. Lett.*

1997, *70* (9), 1143–1145.

(15) Zhang, J.; Ma, X.; Zhang, L.; Lu, Z.; Zhang, E.; Wang, H.; Kong, Z.; Xi, J.; Ji, Z. Constructing a Novel n–p–n Dual Heterojunction between Anatase TiO 2 Nanosheets with Coexposed {101}, {001} Facets and Porous ZnS for Enhancing Photocatalytic Activity. *J. Phys. Chem. C* . **2017**, *121*, 6133–6140.

(16) Tie, L.; Sun, R.; Jiang, H.; Liu, Y.; Xia, Y.; Li, Y. Y.; Chen, H.; Yu, C.; Dong, S.; Sun, J.; Sun, J. Facile Fabrication of N-Doped ZnS Nanomaterials for Efficient Photocatalytic Performance of Organic Pollutant Removal and H2 Production. *J. Alloys Compd.* **2019**, *807*, 151670.

(17) Zheng, X.; Wang, K.; Huang, Z.; Liu, Y.; Wen, J.; Peng, H. MgO Nanosheets with N-Doped Carbon Coating for the Efficient Visible-Light Photocatalysis. *J Ind Eng Chem.* **2019**, *76*, 288–295.

(18) Hsu, C. W.; Li, C. H.; Zhang, L.; Lu, S. Y. N-Doped Carbon Dots@layer Facilitated Heterostructure of TiO2 Polymorphs for Efficient Photoelectrochemical Water Oxidation. *J Taiwan Inst Chem Eng.* **2018**, *93*, 388–396.

(19) Poornaprakash, B.; Chalapathi, U.; Poojitha, P. T.; Vattikuti, S. V. P.; Reddy, M. S. P. (Al, Cu) Co-Doped ZnS Nanoparticles: Structural, Chemical, Optical, and Photocatalytic Properties. *J. Mater. Sci.: Mater. Electron.* **2019**, *30*, 9897–9902.

(20) Jing, M.; Chen, Z.; Li, Z.; Li, F.; Chen, M.; Zhou, M.; He, B.; Chen, L.; Hou, Z.; Chen, X. Facile Synthesis of ZnS/N,S Co-Doped Carbon Composite from Zinc Metal Complex for High-Performance Sodium-Ion Batteries. *ACS Applied Materials and Interfaces* **2018**, *10*, 704–712.

(21) Patterson, A. L. The Scherrer Formula for X-Ray Particle Size Determination. *Phy. Rev.* **1967**, *1*, 5–24.

(22) Tauc, J. Optical Properties and Electronic Structure of Amorphous Ge and Si. *Materials Res. Bull.* **1968**, *3*, 37–46.

(23) Wan, H.; Xu, L.; Huang, W. Q.; Huang, G. F.; He, C. N.; Zhou, J. H.; Peng, P. Band Engineering of ZnS by Codoping for Visible-Light Photocatalysis. *Appl. Phys. A* **2014**, *116*, 741–750.

(24) Sharma, M.; Jain, T.; Singh, S.; Pandey, O. P. Photocatalytic Degradation of Organic Dyes under UV–Visible Light Using Capped ZnS Nanoparticles. *Solar Energy* **2012**, *86*, 626–633.

(25) Ishibashi, K. I.; Fujishima, A.; Watanabe, T.; Hashimoto, K. Detection of Active Oxidative Species in TiO_2 Photocatalysis Using the Fluorescence Technique. *Electrochem. Commun.* **2000**, *2* (3), 207–210.

(26) Chen, C.; Zhao, W.; Li, J.; Zhao, J.; Hidaka, H.; Serpone, N. Formation and Identification of Intermediates in the Visible-Light-Assisted Photodegradation of Sulforhodamine-B Dye in Aqueous TiO_2 Dispersion. *Environ. Sci. Technol.* **2002**, *36* (16), 3604–3611.

(27) Chauhan, R.; Kumar, A.; Pal Chaudhary, R. Photocatalytic Degradation of Methylene Blue with Cu Doped ZnS Nanoparticles. *J. Lumin.* **2014**, *145*, 6–12.

(28) Petrowsky, M.; Frech, R. Temperature Dependence of Ion Transport : The Compensated

Arrhenius Equation. **2009**, 5996–6000.

(29) Bhattacharya, S.; Chakravorty, D. Electrical and Magnetic Properties of Cold Compacted Iron-Doped Zinc Sulfide Nanoparticles Synthesized by Wet Chemical Method. *Chem. Phys. Lett.* **2010**, *444*, 319–323.

(30) Agrawal, N.; Sarkar, M.; Chawda, M.; Ganesan, V. Carrier Induced Magnetism in Dilute Fe Doped Ge_{1-x} Sb_x Thin Films. *Mater. Chem. Phys.* **2013**, *143*, 330–335.